Geophysical Journal International
March 2009, Volume 176, Issue 3, Pages 980 - 994
http://dx.doi.org/10.1111/j.1365-246X.2008.04021.x

Seismic evidence for plume-derived volcanism during formation of the continental margin in southern Davis Strait and northern Labrador Sea

Joanna Gerlings[1, 2, *], Thomas Funck[2], H. Ruth Jackson[3], Keith E. Louden[4] and Frauke Klingelhöfer[5]

[1] University of Copenhagen, Niels Bohr Institute, Blegdamsvej 17, 2100 Copenhagen Ø, Denmark.
[2] Geological Survey of Denmark and Greenland (GEUS), Øster Voldgade 10, 1350 Copenhagen K, Denmark
[3] Geological Survey of Canada, PO Box 1006, Dartmouth, Nova Scotia, B2Y 4A2, Canada
[4] Department of Oceanography, Dalhousie University, Halifax, Nova Scotia, B3H 4J1, Canada
[5] Department of Geodynamics and Geophysics, IFREMER, Centre de Brest, BP 70, 29280 Plouzané, France

*: Corresponding author : J. Gerlings, email address : jgerlings@dal.ca

Abstract:

The crustal structure in the southern Davis Strait and the adjacent ocean–continent transition zone in NE Labrador Sea was determined along a 185-km-long refraction/wide-angle reflection seismic transect to study the impact of the Iceland mantle plume to this region. A P-wave velocity model was developed from forward and inverse modelling of dense airgun shots recorded by ocean bottom seismographs. A coincident industry multichannel reflection seismic profile was used to guide the modelling as reflectivity could be identified down to Moho. The model displays a marked lateral change of velocity structure. The sedimentary cover (velocities 1.8–3.9 km s^{-1}) is up to 4 km thick in the north and thins to 1 km in the south. The segment of the line within southern Davis Strait is interpreted to be of continental character with a two-layered 13-km-thick crust with P-wave velocities of 5.6–5.8 and 6.4–6.7 km s^{-1} in the upper and lower crust, respectively. The crust is underlain by a 2- to 4-km-thick high-velocity layer (7.5 km s^{-1}). This layer we interpret as underplated material related to the Iceland plume. The southern segment of the line in Labrador Sea displays a 2-km-thick layer with a velocity of 4.5 km s^{-1}. This layer can be correlated to a well about 100 km to the west of the line, where Palaeocene basalts and interbedded sediments were drilled. Underneath is a 12-km-thick crust with a 2-km-thick upper layer (5.8–6.6 km s^{-1}) and a 10-km-thick lower layer (6.8–7.2 km s^{-1}). This crust is interpreted to be of oceanic character. S-wave modelling yields a Poisson's ratio of 0.28 for the lower crust, compatible with a gabbroic composition. The igneous crust is 5 km thicker than normal oceanic crust. We suggest that the increased magma production was created by buoyancy-driving flow. We propose a model in which initial seafloor spreading occurred between Labrador and West Greenland, when the Iceland plume arrived in the area at ~62 Ma and caused enhanced magma production. Shortly afterwards (chron 27–26), plume material was channelled southward underplating part of Davis Strait and forming basaltic flows interbedded with sediment.

Keywords: Continental margins: divergent • Continental margins: transform • Hotspots • Crustal structure

1 INTRODUCTION

The crustal structure of southern Davis Strait and northern Labrador Sea was determined along two refraction/wide-angle reflection (R/WAR) seismic lines during the NUGGET (NUnavut to Greenland GEophysical Transect) experiment in 2003 (Fig. 1). Results from Line 1 are published in Funck et al. (2007). This paper will analyze Line 2, which is 185 km long and runs from southern Davis Strait into the northernmost part of Labrador Sea. In addition to the refraction seismic data, coincident reflection seismic data were made available for the analysis courtesy of TGS NOPEC. The composition of the crust in Davis Strait is disputed. Chalmers & Pulvertaft (2001) suggested that Davis Strait primarily consists of continental crust, while Tucholke & Fry (1985) interpreted the crust as mostly oceanic. The southern end of the line in Labrador Sea lies in a region that has

been interpreted as oceanic (Chalmers & Laursen 1995), though just north is a region that extends into Davis Strait, which has been interpreted as a transition zone (Chalmers & Laursen 1995) with an uncertain affinity between oceanic and continental crust (Fig. 2). The Davis Strait region is also of interest because of evidence of Paleocene volcanic rocks associated with the arrival of the Iceland mantle plume beneath the Greenland lithosphere (Storey et al. 1998). Seaward-dipping reflections close to Line 2 (Chalmers & Laursen 1995) suggest a volcanic style continental margin in the northernmost Labrador Sea, while the transition zone in southern Labrador Sea was interpreted to consist of serpentinized mantle (Chian & Louden 1994), which is characteristic of non-volcanic continental margins. The objectives of the NUGGET refraction seismic experiment were to (i) determine the nature of the crust in the southern Davis Strait, (ii) to characterize the composition of the transitional crust in the northern Labrador Sea, and (iii) to look for evidence for interaction between the Iceland plume and the transform-rifted margin in Davis Strait.

2 GEOLOGICAL SETTING

Davis Strait lies between Greenland and Baffin Island and separates Baffin Bay in the north from Labrador Sea in the south. The onset of rifting between Labrador and Greenland occurred in the Early Cretaceous (140 Ma; Larsen 2006). The much later onset of seafloor spreading did not begin until the Late Cretaceous or Early Paleogene. Roest & Srivastava (1989a) proposed chron 33 (79.5-73.6 Ma; time scales are taken from Ogg and Smith (2004)) to be the oldest magnetic anomaly in Labrador Sea and hence the onset of seafloor spreading. Chian et al. (1995) suggest that the seafloor spreading began

sometime between chrons 31 (71-67.8 Ma) and 27 (63.1-61.7 Ma) while Chalmers (1991) interpreted the oldest magnetic anomaly in Labrador Sea as chron 27n (62-61.7 Ma). There is some discrepancy in the interpretation of the magnetic data in northern Labrador Sea. Fig. 2 shows the mismatch of the interpretation of the magnetic anomalies of Roest & Srivastava (1989b) and of Chalmers and Laursen (1995). Just south of Davis Strait, the discrepancy in the interpretation of the magnetic anomalies is greatest. Further south there is a general agreement up to magnetic anomaly 27.

The Ungava Fault Zone (UFZ) marks the NW termination of oceanic crust in Labrador Sea. The position of the UFZ is assumed to be coincident with a positive gravity anomaly and a weak positive magnetic anomaly that run from the southeastern tip of Baffin Island to the northern part of Davis Strait (Chalmers & Pulvertaft 2001). This structural zone has been interpreted as part of the transform system linking seafloor spreading in Labrador Sea with spreading in Baffin Bay (Rice & Shade 1982). The UFZ was the main transform structure in northern Labrador Sea and Davis Strait during Paleocene spreading, but during Eocene spreading, movement between the North American and Greenland plates was probably also transferred along the Hudson Fracture Zone (HFZ; Chalmers & Pulvertaft 2001).

Two major pulses of volcanism have been identified by Storey et al. (1998) in West Greenland. Paleogene volcanism at ~61 Ma may be associated with the Icelandic plume and Early Eocene volcanism was probably a result of the reorientation of the spreading direction in Labrador Sea at chron 24r (56.7-53.8 Ma), when seafloor spreading began between Europe and Greenland (Srivastava 1978). Seafloor spreading in Labrador Sea ended during chron 13 (34.8-33.3 Ma; Roest & Srivastava 1989a).

3 WIDE-ANGLE SEISMIC EXPERIMENT

3.1 Data acquisition and processing

Line 2 is oriented in a NNW-SSE direction and a total of 15 ocean bottom seismometers (OBS) owned by Ifremer (Institut français de recherche pour l'exploitation de la mer) were deployed along the line with an average spacing of 12 km. The energy source used in this survey was a tuned airgun array that consisted of 12 guns (2.0 to 16.4 L) with a total volume of 104 L. The average shot spacing was 146 m. The Global Positioning System (GPS) was used for navigation and timing.

OBS data were converted to SEGY format, debiased, and corrected for the drift of the OBS clock. Positions of the OBS at the seafloor were determined from travel time picks of the direct wave. Strong tidal currents in the study area caused relatively high noise levels in the frequency range 2-4 Hz. The main seismic energy lies in the window from 5 to 10 Hz, whereas for close offsets also frequencies in the 10 to 18 Hz range were observed. For the record sections shown in this paper (Figs. 3 to 5 and 7) a 5 to 10 Hz bandpass filter was used. Trace amplitudes in the seismograms were weighted by their distance to the OBS to increase amplitudes with increasing offset. Water depths along Line 2 were obtained from the coincident MCS profile (GreenCan Line 02-01 collected by TGS NOPEC). The MCS profile was acquired with a 6-km-long streamer with 480 channels.

3.2 Methodology

The instrument positions were projected onto a baseline that consisted of two great circle arcs – from the northern end of the line to the cross point with Line 1, and from there to the southern end of Line 2. The *P*-wave velocity model for the crust and upper mantle was developed using the program RAYINVR (Zelt & Smith 1992; Zelt & Forsyth 1994). Initially, a forward model was developed from top to bottom by fitting the observed travel times. Then the velocities within the layers were optimized by using the inversion algorithm. Synthetic seismograms and the coincident MCS data were then used for a final adjustment the velocity model. The layer geometry down to the basement was mainly defined by the coincident MCS profile.

3.3 Wide-angle seismic data

Some of the key features of the velocity structure along Line 2 are illustrated in Figs. 3 to 5. Phase names of the refractions and reflections are summarized in Table 1. OBS 4 (Fig. 3) shows a change in the signature from north to south. The crustal refractions P_{c1} and P_{c2} with phase velocities of 5.6 km/s and 6.4 km/s, respectively, can be seen north of the OBS. South of the OBS, a refraction (P_{L2}) with a phase velocity of 5.8 km/s is observed between offsets of 5 to 20 km. A time delay in the first arrivals (time gap of 0.2 sec.) occurs 20 km south of the OBS, which indicates a low velocity zone (LVZ). The mantle refraction (P_{n2}) with a phase velocity of 8.1 km/s (offset 60 to 90 km) is seen in this section as well as the $P_{m1}P$ reflection from the base of the crust (offset 15 to 45 km, clearest signal in the north) and a reflection P_zP in the upper mantle (offset >110 km). Furthermore, a crustal reflection ($P_{c1}P$) is recorded north of the OBS between offsets of 10 to 20 km.

On OBS 8 (Fig. 4) P_{L2} is observed for offsets <20 km. A crustal refraction P_{L3} with a velocity of 6.8 km/s is identified to the south of the OBS for offsets >20 km. On this section there is a very sharp and high-amplitude signal from the P_zP phase at offsets between 50 and 80 km. The identification of first arrivals north of station 8 is more difficult due to higher noise levels than in the previous sections. The reflections $P_{m1}P$ and $P_{m3}P$ are observed between 10 to 30 km north and between 30 to 70 km south, respectively. The $P_{m2}P$ reflection was only observed on OBS 7 and 9.

On OBS 14 (Fig. 5), refractions P_{L2}, P_{L3} and P_{n2} are observed, as well as the reflections $P_{m3}P$ and P_zP. Furthermore, a refraction P_{s6} with a phase velocity of 4.4 km/s is observed. All these arrivals have a high signal-to-noise ratio. P_{L2} is observed for offsets of 10 to 30 km, P_{L3} for offsets of 30 to 90 km, and P_{n2} at offsets >110 km. $P_{m3}P$ is observed at offsets of 40 to 80 km and P_zP for offsets of 35 to 120 km.

4 RESULTS

4.1 *P*-wave velocity model

The *P*-wave velocity model for NUGGET Line 2 is shown in Fig. 6. The line displays a marked lateral change in velocity structure. The sedimentary cover with velocities of 1.8 to 3.9 km/s is up to 4 km thick in the north and thins to 1 km in the south. South of 50 km in the model, a layer with a velocity of 4.4 km/s is found beneath the sediments. This layer thickens from 1 km in the north to 2 km in the south. Later, we will interpret this layer to consist of Paleogene basalts, possibly interbedded with sediments.

In the northern part of Line 2, the crystalline crust is up to 13 km thick and is interpreted as thinned continental crust. The crust is divided into two layers, upper and lower continental crust, with *P*-wave velocities of 5.6 km/s to 5.8 km/s and 6.4 km/s to 6.7 km/s, respectively. The velocity structure changes to the south, where a 2-km-thick upper crustal layer and a 10-km-thick lower crustal layer were found. The upper crustal layer has a high velocity gradient with a velocity of 5.8 km/s at the top and 6.6 km/s at the base. Lower crustal velocities range between 6.8 km/s and 7.2 km/s. Thickness, velocities and velocity gradient of the upper layer are very characteristic for oceanic layer 2 and velocities in the lower layer are compatible with oceanic layer 3 (White et al., 1992). This will be discussed later in more detail. The southward dipping boundary between the two types of crust is mapped by reflections ($P_{m3}P$) that are associated with the impedance contrast across the boundary. Underneath the continental crust is a 2 to 4 km thick layer with a velocity of 7.5 km/s, which is interpreted as formed by magmatic underplating. The Moho shallows from 20 km in the north to 17 km in the south. The velocity in the upper mantle is 8.1 km/s. The P_zP reflections were modeled by introducing an upper mantle reflector that varies in depth from 28 km in the north to 24 km in the south. However, no refractions were observed in the records that could have determined the velocity beneath this reflector. The velocity model shows two LVZs. The first one is associated with a thin sliver of oceanic layer 2 and possibly some overlying basalt flows that overlies the continental crust between 50 and 90 km. The second LVZ can be found between 90 and 120 km where lower continental crust is overlain by oceanic layer 3.

4.2 *S*-wave velocity model

The quality of *S*-wave arrivals was very poor except for phases within oceanic layer 3 (S_{L3} and S_mS) (Fig. 7). The *S*-wave velocity at the top of layer 3 was modeled with 3.75 km/s, which together with the *P*-wave velocity of 6.8 km/s gives a Poisson's ratio of 0.28.

4.3 Model uncertainty and resolution

The assigned pick uncertainty, the RMS (root-mean-square) travel time residual, the number of travel time picks for individual *P*- and *S*-phases and the normalized χ^2 are summarized in Tables 2 and 3. Pick uncertainties are indicated in Fig. 8. The expectation value of the normalized χ^2 is 1 (Bevington & Robinson 2003). Our results show a good agreement between observed and calculated travel times. The normalized χ^2 is 0.908 for the *P*-phases and 1.064 for the *S*-phases. Fig. 6 represents the diagonal of the resolution matrix of the velocity model. Resolution matrix diagonals > 0.5 are said to be well-resolved model parameters (Lutter & Nowack 1990; Zelt 1999). Resolution is good within the crust except in the LVZ where the continental crust is overlain by oceanic crust and no refractions are observed.

A comparison of the ray coverage with the resolution matrix (Fig. 6) shows that the area with no ray coverage is poorly resolved as expected. The resolution within the sedimentary layers is reduced compared to the crust, which is related to the lack of reversed observations in the thin sediment layers. The MCS data compensate partly for the lack of these reversed observations. Zones in the mantle that are sampled by rays show an acceptable resolution. The velocity resolution within the underplated layer is

mostly < 0.5, but both top and bottom of the layer are sampled by a number of $P_{m1}P$ and $P_{m2}P$ reflections. The resolution for the basalt layer is acceptable south of 100 km but farther north very few refractions were observed.

To determine the uncertainty of the velocity and layer boundaries, selected nodes in the model were perturbed to check for the sensitivity of the travel times on these changes. The velocity uncertainty in the crust is ±0.10 km/s, and ±0.20 km/s in the underplated layer and upper mantle. The depth uncertainty of the layer boundaries is ±1.0 km. The sensitivity of the Poisson's ratio in oceanic layer 3 upon perturbation was tested as well. This showed that the Poisson's ratio has an uncertainty of ± 0.01.

4.4 The gravity model

Two-dimensional gravity modeling was carried out using the Talwani algorithm (Talwani et al. 1959), primarily to check the velocity model for consistency with the gravity data. Free-air gravity data were extracted from Oakey et al. (2001). The gravity model was obtained from conversion of *P*-wave velocities to density using the empirical relationship of Ludwig et al. (1970), which can be approximated by

$$\rho = -0.00283v^4+0.0704v^3-0.598v^2+2.23v-0.7$$

where v is *P*-wave velocity in km/s and ρ is density in Mg/m^3. The mantle was modeled with a density of 3.30 Mg/m^3. The model was extended 300 km in each direction to minimize edge effects. The theoretical gravity profile computed from the *P*-wave velocity model is shown in Fig. 6. The lateral change in velocity structure in the middle of the

profile is also visible in the gravity signal. In the south, the free-air gravity anomaly is ca. 10 mGal and decreases to -20 mGal in the north. An approximate match between observed and calculated gravity was achieved. The largest misfit is observed between 0 and 40 km, and south of 160 km. Fig. 9 shows the regional gridded gravity. The gravity does not change significantly perpendicular to Line 2, which suggest that the two-dimensional modeling approach is justified. The largest misfits between observed and calculated gravity occur at either end of the line. This is attributed to the reduced ray overage in these zones and to deviations from the horizontal extension of the density model outside the line.

5 DISCUSSION

The velocity model (Fig. 6) shows four main features: oceanic crust in the southern end of Line 2, basalt overlying the oceanic crust, continental crust in the northern end of Line 2, and an underplated layer at the base of the continental crust. Fig. 10 is an updated version of Chalmers & Pulvertaft's (2001) geological map (Fig. 2) that includes the results of NUGGET Line 1 (Funck et al. 2007) and Line 2. In the following sections, we will discuss the oceanic crust in northern Labrador Sea, the nature of the continental crust in Davis Strait, and the effect of the plume on the formation of the continental margin.

5.1 Oceanic crust in northern Labrador Sea

The crust in the southern part of Line 2 can be divided into two layers (layer 2 and 3) with a velocity structure similar to normal oceanic crust. Layer 2 is 2-km-thick and has

a high velocity gradient (0.4 s^{-1}) from 5.8 km/s at the top to 6.6 km/s at the bottom. The velocity increases slightly to 6.8 km/s at the top of layer 3 and the gradient decreases to 0.04 s^{-1}. Fig. 11 shows the velocity-depth curve from the southern part of Line 2 in comparison with the range of velocity-depth curves for 59 to 127 Ma old oceanic crust in the Atlantic Ocean (White et al. 1992). The southern part of Line 2 fits into the range of the velocity profile, with the exception of the thickness of oceanic layer 3. Oceanic layer 3 on Line 2 is 10 km thick, which is 5 km more than average. However, the velocity gradient on Line 2 is similar to average values for layer 3. A thickening of oceanic layer 3 is consistent with refraction models from the Reykjanes Ridge (SSW of Iceland) where there is similar thickening of layer 3 of up to 8 km (Smallwood & White 1998). Smallwood & White (1998) propose that this is due to increased temperatures in the mantle which relates to pulses from the Iceland plume that have been channeled southward.

Only few *S*-wave observations were made on Line 2, but they confirm the gabbroic composition of the lower crustal layer in the south. With a *P*-wave velocity of 6.8 km/s and *S*-wave velocity of 3.75 km/s, the Poisson's ratio is 0.28±0.01, which is consistent with gabbro (Holbrook et al. 1992). In contrast, serpentinized mantle as found in the continent-ocean transition zone in southern Labrador Sea (Chian & Louden 1994) does not match the observed *P* and *S*-wave velocities on Line 2.

Louden et al. (2004) have compiled a thickness map for the oceanic crust of the North Atlantic that shows increased values for the southern part of Line 2. This local high is uncharacteristic for Labrador Sea but is compatible with the total crustal thickness of 14 km observed on Line 2 (including the additional 2 km of basalts on top). We propose

that the extra 5 km of oceanic layer 3 may be the result of active mantle upwelling possibly related to the Iceland plume. The crustal velocity and thickness of Line 2 suggest active upwelling (Korenaga et al. 2002). There is also the possibility that extra crust was added later on but the velocity model and the MCS data do not show a divided lower crust. If the thick oceanic crust on Line 2 correlates with the thick crust identified by Louden et al. (2004), we can use the map of Louden et al. (2004) to trace the regional extent of the thick crust. The thick crust covers a small region, which extends southwards to about 61.5°N (Fig. 10). Note that the northern limit of this region could not be mapped by Louden et al. (2004) beyond the border of NUGGET Line 1.

The southern end of Line 2 is located in a region that Chalmers and Laursen (1995) interpreted to be of oceanic character, which is consistent with the interpretation of the velocity model for Line 2 (Figs. 2 and 10). The coverage of magnetic data in this region is poor, which has resulted in conflicting interpretations of magnetic anomalies (Roest & Srivastava 1989b; Chalmers & Laursen 1995). Using the Roest & Srivastava (1989b) interpretation, the southern half of Line 2 is located landward of anomaly 27 (63.1-61.7 Ma, Fig. 12) and partly landward of magnetic anomaly 31 (71-67.8 Ma). Chalmers (1991) and Chalmers & Laursen (1995) interpretations locate Line 2 between magnetic anomaly 27 and 26 (63.1-61.7 Ma and 61.7-58.4). Storey et al. (1989) have suggested that the Iceland plume arrived beneath the Greenland lithosphere at ~62 Ma and that the initial volcanism from the plume occurred at 61.3-60.9 Ma in the region. If our interpretation is right that the thick oceanic crust at the southern end of Line 2 is related to the Iceland plume, then there is a good agreement with the interpretation of magnetic anomalies by Chalmers and Laursen (1995). Using the Roest and Srivastava

(1989b) interpretation, the thick oceanic crust on Line 2 should have formed before anomaly 31 but there is no onshore evidence for volcanism of that age. This is why we lean towards Chalmers' and Laursen's (1995) interpretation of magnetic anomalies in the northernmost Labrador Sea. However, our data cannot confirm that anomaly 27 is the oldest magnetic anomaly in that area as suggested by Chalmers and Laursen (1995). This is due to our line location parallel to the margin, which prevents the detection of the continent-ocean boundary.

5.2 Continental crust and underplating in Davis Strait

The nature of the crust in Davis Strait has been controversial. Tucholke & Fry (1985) suggested that most of the crust in Davis Strait is oceanic while Chalmers & Pulvertaft (2001) considered that the crust is mostly continental (Fig. 2). Srivastava & Roest (1999) proposed a propagating rifting model for the initial opening of Labrador Sea. Their rifting process results in a complex model with regions of oceanic crust of different ages. Srivastava & Roest (1999) have delinated a boundary from gravity data, which divides the ocean crust into a northern and southern part. This boundary they call the western boundary (Figs. 2 and 10; Srivastava & Roest 1999). Our results from the NUGGET experiment show that the oceanic crust in Labrador Sea does not extend northward across this boundary. We interpret the crust north of Srivastava & Roest's (1999) western boundary to be of continental character. The *P*-wave velocities of the crust in the northern part of Line 2 (5.6 to 6.7 km/s), which lies in the southern part of Davis Strait, are slightly lower than the velocity of oceanic crust (5.8 to 7.2 km/s) found in the south. In addition, the northern crustal domain on Line 2 is intersected by Line 1,

where the crust in that segment is interpreted to be of continental character that can be followed to the coast of Greenland (Funck et al. 2007; Fig. 1). Hence we agree with Chalmers & Pulvertaft (2001) that southern Davis Strait is mostly of continental character.

Chalmers (1997) suggests that the continental crust in southern Davis Strait is underlain in some places by transitional crust (Fig. 2), composed of serpentinized mantle. We, however, find that the continental crust has been underplated with magmatic material (Figs. 6 and 10). Underplating with velocities of 7.4-7.5 km/s is also observed in the centre part of Line 1 (Funck et al. 2007) and can be correlated to the underplating with velocities of 7.5-7.6 km/s on Line 2. The difference in the crustal velocities in what we interpret as the underplated layer (7.5-7.6 km/s) and the lower oceanic crust (6.8-7.2 km/s) indicate that higher mantle temperatures were needed to create the underplating and that the melt of the underplate is different than that of the thick oceanic crust farther south. The melt that created the additional oceanic crust came from a potentially complicated system, where the material interacted with the spreading system. Potentially, this could create a mixture between the two melts that is different from the north, where the material is only related to the initial melt from the plume.

Picrites, high temperature melt rocks (1480°C; Mckenzie & Bickle 1988), have been found northeast of the NUGGET lines on Disko Island in northern Davis Strait (Larsen et al. 1992). The picrites (63 Ma) were formed at the same time as the arrival of the mantle plume (Larsen et al. 1992) and may be comparable to the high temperature melt of underplating. High temperature picritic melts associated with continental flood basalts are derived from hot, plume-source mantle at the plume axis (Campbell &

Griffiths 1990). The reason why the volcanism began west of Greenland could be related to the presence of pre-existing regions with thin lithosphere that may control the location of volcanism over a plume (Larsen et al. 1992; Thomson & Gibson 1991; Nielsen et al. 2002). This may suggest that the underplating on Line 2 is related to the arrival of the Iceland plume in the Davis Strait area and southward channeling of plume material along the base of the lithosphere.

5.3 Volcanism in southern Davis Strait

In 1977 the Bundesanstalt für Geowissenschaften und Rohstoffe (BGR) conducted a regional seismic survey in Labrador Sea. Some of these lines have been reprocessed and reinterpreted (Chalmers & Laursen 1995). One line, BGR/77-6, intersects Line 2 south of OBS 10 and near shot-point 5000 on BGR/77-6 (Fig. 1). Chalmers & Laursen (1995) identified seaward-dipping reflections, which are characteristic for volcanic style continental margins, at a depth of 4 to 5.5 s two-way-time (TWT) in the vicinity where Line 2 intersects BGR/77-6 (Fig. 12). In the southern part of MSC GreenCan Line 02-01 (collected by TGS NOPEC coincident with Line 2; Fig. 13) the reflection seismic record shows a series of parallel, horizontal or sub-horizontal high-amplitude reflections between 4 to 5 s TWT, above what is interpreted as oceanic layer 2. These reflections correspond to the seaward-dipping reflections interpreted on BGR/77-6 close to the crossing point with Line 2.

Line 1 crosses the Gjoa G-37 well 100 km to the west of Line 2 (Fig. 1). The well terminates 3 km below sea level in sediments of Maastrichtian age overlain by Paleocene basalts (Klose et al. 1982). This layer with basalt and interbedded sediments has a

velocity of 4.3 km/s on Line 1 (Funck et al. 2007) and can be correlated to Line 2, where it is up to 2 km thick with a velocity of 4.4 km/s. Furthermore, it corresponds to the layer where seaward-dipping reflections were located on BGR/77-6. Therefore, the layer that overlies oceanic layer 2 is interpreted to consist of basalts with possible interbedded sediments.

On basis of these results we propose the following model for the events in southern Davis Strait and northern Labrador Sea (Fig. 14):

(a) Continental rifting was initiated as early as in the Early Cretaceous (140 Ma) between Labrador and West Greenland (Fig. 14a; Larsen 2006) and continued in several phases up to the early Paleocene (Chalmers et al.1993). The rifting was associated with crustal thinning.

(b) Seafloor spreading was initiated shortly before or at the time of the arrival of the Iceland plume (~62 Ma) forming thick oceanic crust (Fig. 14b).

(c) For a brief period during the formation of the earliest ocean crust at chron 27-26, underplating and basalt flows occurred (Fig. 14c). This crust is similar to the East Greenland volcanic margin (Hopper et al. 2003), where thick oceanic crust has been observed with seaward-dipping-reflectors on top.

(d) Seafloor spreading continued forming thick oceanic crust possibly until chron 24. At this time a reorientation of the spreading system occurred when seafloor spreading began between Greenland and Europe (Srivastava 1978). Seafloor spreading slowed in the Labrador Sea after chron 24 and ended by chron 13 (Roeat & Srivastava 1989a; Fig. 14d).

Our interpretation of the velocity model of NUGGET Line 1 and 2 show underplating and basalt flows, which are normally related to a volcanic style continental margin. It most, however, be noted that the profile of Line 2 (Fig. 6) does not give a true picture of the boundary between the oceanic and continental of crust. The profile is oriented nearly perpendicular to the direction of rifting, which means that the apparent dip on the profile is influenced by the geometry relative to the line (Figs. 2 and 10). The boundary between continental and oceanic crust is a sharp contact that is less than 20 km wide, which is more in line with a volcanic margin. However, volcanism that probably postdates the onset of seafloor spreading suggests that this is not a normal volcanic margin. Funck et al. (2007) have proposed the rifting phase was initially non-volcanic and later overprinted by volcanism associated with the Iceland plume. This is consistent with the absence of volcanism in southern Labrador Sea, where serpentinized mantle is found in the continent-ocean transition zone in the Greenland margin (Chian & Louden 1994) and hence interpreted as a non-volcanic margin.

6 CONCLUSIONS

The purpose of NUGGET Line 2 was to determine the composition of the crust south of Davis Strait in answer to the following questions: (i) whether the crust is of continental, transitional, or oceanic character, (ii) whether this is a volcanic or a non-volcanic style continental margin, and (iii) what is the extent of plume material. We draw the following conclusions:

1) The results from NUGGET Line 2 and Line 1 show that the crust in the southern part of Davis Strait is of continental character.

2) The continental crust was underplated by igneous crust that is related to the Iceland plume in the Davis Strait area. The plume material was channeled southward along the base of the thinned lithosphere.
3) Thick oceanic crust found on southern end of Line 2 was created by enhanced mantle flow. The melt that created the additional oceanic crust came from a potentially complex system, where the material was created by interaction of the Iceland mantle plume interacted with the spreading system.
4) On Line 2, 12-km-thick igneous crust and up to 2-km-thick basalt flows are observed. Close by on Line BGR/77-6, seaward dipping reflections were found that correlate with the basalt layer on Line 2. These features are normally characteristic for volcanic-style margins. However, the volcanism postdates the seafloor spreading which makes it possible that the rifting phase was initially non-volcanic but that the later encounter with the Iceland mantle plume resulted in a volcanic-style margin.

7 ACKNOWLEDGMENT

We would like to thank all personnel onboard CCGS Hudson who helped to collect the seismic data. We also thank Jens Christian Olsen from TGS NOPEC for providing the coincident reflection seismic data. The NUGGET project was funded by the Danish National Research Foundation (Danmarks Grundforskningsfond), the Natural Sciences and Engineering Research Council of Canada, and the NEON (New Energy Options for Northerners) program of the Geological Survey of Canada. Part of the OBS

operation was supported by Ifremer and by the European Union through a grant for the 'Access to Large Scale Facilities' at GEOMAR, Kiel, Germany.

8 REFERENCES

Bevington, R.P., & Robinson, D.K., 2003. *Data reduction and error analysis for physical sciences*, 3rd edn, McGraw-Hill, New York.

Campbell, I.H. & Griffiths, R.W., 1990. Implications of mantle plume structure for evolution of flood basalts, *Earth Planet. Sci. Lett.*, 99, 79--93.

Chalmers, J.A., 1991. New evidence on the structure of the Labrador Sea/Greenland continental margin, *Journal of the Geological Society, London*, 148, 899--908.

Chalmers, J.A., Pulvertaft, T.C.R., Christiansen, F.G., Larsen, H.C., Laursen, K.H. & Ottesen, T.G., 1993. The southern West Greenland continental margin: rifting history, basin development, and petroleum potential, *in Petroleum Geology of Northwest Europe: Proceedings of the 4th Conference*, pp. 915--931, ed. Parker, J.R., Geological Society, London.

Chalmers, J.A., & Laursen, K.H., 1995. Labrador Sea: the extent of continental and oceanic crust and the timing of the onset of seafloor spreading, *Marine and Petroleum Geology*, 12, 205--217.

Chalmers, J. A., 1997. The continental margin off southern Greenland: along-strike transition from an amagmatic to a volcanic margin. *Journal of the Geological Society, London,* 154, 571--576.

Chalmers, J.A., & Pulvertaft, T.C.R., 2001. Development of the continental margins of the Labrador Sea: a review, *in Non volcanic rifting of continental margins: a comparison of evidence from land and sea*, pp. 77--105, ed. Wilson, R.C.L., Whitmarsh, R.B., Taylor, B., & Frotzheim, N., Geological Society, London, Special Publications.

Chian, D., & Louden, K., 1994. The continent-ocean crustal transition across the southwest Greenland margin, *J. Geophys. Res.*, 99, 9117--9135.

Chian, D., Keen, C., Reid, I., & Louden, K., 1995. Evolution of nonvolcanic rifted margins: New results from the conjugate margins of the Labrador Sea, *Geology*, 23, 589--592.

Funck, T., Jackson, H.R., Louden, K.E., & Klingelhöfer, F., 2007. Seismic study of the transform-rifted margin in Davis Strait between Baffin Island (Canada) and Greenland: What happens when a plume meets a transform, *J. Geophys. Res.*, 112, B04402, doi:10.1029/2006JB004308.

Holbrook, W.S., Mooney, W.D., & Christensen, N.I., 1992. The seismic velocity structure of the deep continental crust, *in Continental lower crust*, pp. 1--43, ed. Fountain, D.M., Arculus, R., and Kay, R., Elsevier Sci, New York.

Hopper, J.R., Dahl-Jensen, T., Holbrrok, W.S., Larsen, H.C., Lizarralde, D., Korenaga, J., Kent, G.M. & Keleman, P.B., 2003. Structure of the SE Greenland margin form seismic reflection and refraction data: Implications for nascent spreading center subsidence and asymmetric crustal accretion during North Atlantic opening, *J. Geophys. Res.*, 112, doi:10.1029/2002JB001996.

Klose, G.W., Malterre, E., McMillan, N.J., & Zinkan, C.G., 1982. Petroleum exploration offshore southern Baffin Island, northern Labrador Sea, Canada, *in Arctic geology and geophysics*, pp. 233--244, ed. Embry, A.F., & Balkwill, H.R., Canadian Society of Petroleum Geologists, Memoir 8.

Korenaga, J., Kelemen, P. B., & Holbrook W.S., 2002. Methods for resolving the origin of large igneous provinces form crustal seismology, *J. Geophys. Res.*, 107, 2178, doi:10.1029/2001JB001030.

Larsen, L.M., Pedersen, A.K., Perdersen, G.K., & Piasecki, S., 1992. Timing and duration of Early Teriary volcanism in the North Atlantic: new evidence from West Greenland, *in Magmatism and the Causes of Continental Break-up,* pp. 321--333, ed. Storey, B.C., Alabaster, T., & Pankhurst, R.J., Geological Society, Special Publications.

Larsen, L.M., 2006. Mesozoic to Palaeogene dyke swarms in West Greenland and their significance for the formation of the Labrador Sea and the Davis Strait, Geological Survey of Denmark and Greenland, *Report 2006/34*, 69 pp.

Louden, K.E., Tucholke, B.E., & Oakey, G.N., 2004. Regional anomalies of sediment thickness, basement depth and isostatic crustal thickness in the North Atlantic Ocean, *Earth Planet. Sci. Lett.*, 224, 193--211.

Ludwig, W.J., Nafe, J.E., & Drake, C.L., 1970. Seismic refraction, *in The sea*, pp. 53--84, ed. Maxwell, A.E., Wiley-Interscience, New York.

Lutter, W.J., & Nowack, R.L., 1990. Inversion for crustal structure using reflections from the PASSCAL Ouachita Experiment, *J. Geophys. Res.*, 95, 4633--4646.

McKenzie, D. & Bickle, M.J., 1988. The volume and composition of melt generated by extension of lithosphere, *Journal of Petrology*, 29, 625--679.

Nielsen, T.K., Larsen, H.C., & Hopper, J.R., 2002. Contrasting rifted margin styles south of Greenland: implications for mantle plume dynamics, *Earth Planet. Sci. Lett.*, 200, 271--286.

Oakey, G.N., Forsberg, R., & Jackson, H.R., 2001. Gravity anomaly map, bouguer on land, free air at sea, Davis Strait region, Canadian and Greenland Arctic, *Open File Rep. 3934B*, Geological Survey of Canada, Ottawa, Ontario.

Ogg, J.G., & Smith, A.G., 2004. The geomagnetic polarity time scale, *in A geologic time scale 2004*, pp. 63--86, ed. F.M. Gradstein, J.G. Ogg, & A.G. Smith., Cambridge University Press, Cambridge, England.

Rice, P.D. & Shade, B.D., 1982. Reflection seismic interpretation and seafloor spreading history of Baffin Bay, *in Arctic Geology and Geophysics*, pp. 245--265, ed. Embry, A.F. & Balkwill, H.R., Canadian Society of Petroleum Geologists, Memoirs, 8.

Roest, W.R., & Srivastava, S.P., 1989a. Sea-floor spreading in the Labrador Sea: A new reconstrution, *Geology*, 17, 1000--1003.

Roest, W.R., & Srivastava, S.P., 1989b. Sea-floor spreading history I Labrador Sea, Magnetic anomalies along track, Scale 1:2.000.000, *in East Coast Basin Atlas Series. Labrador Sea*, pp 98. Coordinator Bell, J.S., Geological Survey of Canada, Atlantic Geoscience Centre, Dartmouth, Nova Scotia.

Smallwood, J.R., & White, R.S., 1998. Crustal accretion at the Reykjanes Ridge, 61°-62°N, *J. Geophys. Res.*, 103, 5185--5201.

Srivastava, S.P., 1978. Evolution of the Labrador Sea and its bearing on the early evolution of the North Atlantic, *Geophysical Journal of the Royal Astronomical Society*, 52, 313--357.

Srivastava, S.P., & Roest, W.R., 1999. Extent of oceanic crust in the Labrador Sea, *Marine and Petroleum Geology*, 16, 65--84.

Storey, M., Duncan, R.A., Pedersen, A.K., Larsen, L.M., & Larsen, H.C., 1998. 40Ar/39Ar geochronology of West Greenland tertiery volcanic providence, *Earth Planet. Sci. Lett.*, 160, 569--586.

Talwani, M., Worzel, J.L., & Landisman, M., 1959. Rapid gravity computation for two-dimensional bodies with application to the Mendocino submarine fracture zone, *J. Geophys. Res.*, 64, 49--59.

Thomson, R.N. & Gibson, S.A., 1991. Subcontinental mantle plumes, hotspots and pre-existing thinspots, *Journal of Geological Society, London*, 148, 973--977.

Tucholke, B.E., & Fry, V.A., 1985. Basement structure and sediment distribution in Northwest Atlantic Ocean, *American Association of Petroleum Geologists Bulletin*, 69, 2077--2097.

White, R.S., McKenzie, D., & O'Nions, R.K., 1992. Oceanic crustal thickness from seismic measurements and rare earth element inversions, *J. Geophys. Res.*, B13, 19 683 -- 19 715.

Zelt, A.C., & Smith R.B., 1992. Seismic travel time inversion for 2-D crustal velocity structure, *Geophys. J. Int.*, 108, 16--34.

Zelt, A.C., & Forsyth, D.A., 1994. Modeling wide-angle seismic data for crustal structure: southeastern Greenville Province, *J. Geophys. Res.*, 99, 11,687--11,704.

Zelt, A. C., 1999. Modeling strategies and assessments for wide-angle seismic travel time data, *Geophys. J. Int.*, 139, 183--204.

Figure 1: Location map of the NUGGET experiment and Line BGR/77-6. TGS-NOPEC GreenCan Line 02-01 is coincident with NUGGET Line 2. Magnetic anomalies 24-31 are shown as thin dashed lines, extinct spreading center and faults are shown as gray lines (Roest & Srivastava 1989b). Depth contours are shown for 1000 m, 2000 m, and 3000 m. Upper left corner: location of OBS on Line 2 and part of Line 1. Upper right corner: Regional location of the NUGGET experiment.

Figure 2: Geological map of Davis Strait and Labrador Sea. Modified from Chalmers and Pulvertaft (2001). See legend for identification of map features. Note that an updated version based on results from this paper is shown in Fig. 10.

Figure 3: Record section (top) with computed travel times and ray path diagram (bottom) for the vertical geophone of OBS 4. The vertical scale for the record section is travel time (s) using a reduction velocity of 6.5 km/s, and the horizontal scale is shot-receiver distance (offset in km). The horizontal scale in the ray path diagram is distance (km) along the velocity model. The phases are described in the text. The top right corner shows a blow up of the record section between 0-40 km offset and 2-6 seconds. The arrow marks the delay in arrival times associated with the LVZ.

Figure 4: Record section (top) with computed travel times and ray path diagram (bottom) for the vertical geophone of OBS 8. The vertical scale for the record section is travel time (s) using a reduction velocity of 6.5 km/s, and the horizontal scale is shot-receiver distance (offset in km). The horizontal scale in the ray path diagram is distance (km)

along the velocity model. The phases are described in the text. Despite the generally high signal-to-noise ratio, the section has increased ’wrap around’ noise between -130 and -90 km from previous shots. However, it is still possible to correlate some seismic energy within the noise.

Figure 5: Record section (top) with computed travel times and ray path diagram (bottom) for the vertical geophone of OBS 14. The vertical scale for the record section is travel time (s) using a reduction velocity of 6.5 km/s, and the horizontal scale is shot-receiver distance (offset in km). The horizontal scale in the ray path diagram is distance (km) along the velocity model. The phases are described in the text.

Figure 6: *P*-wave velocity model (middle) along Line 2. Numbers indicate velocity in km/s and numbers in brackets indicate the density in Mg/m^3. Triangles mark the location of the OBS used for the modeling. Wide-angle reflection interfaces are marked with bold grey lines. The vertical lines near OBS 5 and 10 show the position of the cross point with Line 1 and line BGR/77-6, respectively. Ray coverage of the *P*-wave velocity model is indicated by light shading. The *P*-wave velocity model was converted to density using the velocity-density relationship of Ludwig et al. (1970). The calculated gravity is compared to the observed gravity (top) from Oakey et al. (2001), shown in Fig. 9. Diagonal values of the resolution matrix of the *P*-wave velocity model (bottom). The values for the velocity nodes have been contoured. Values >0.5 indicate a good resolution.

Figure 7: Record section with computed travel times of *S*-waves for vertical geophones of OBS 10 and 14. The vertical scale of the record section is the travel time (s) using a reduction velocity of 3.8 km/s, and the horizontal scale is shot-receiver distance (offset in km).

Figure 8: Comparison of observed and calculated travel times for OBS 1-15 shown together with the corresponding ray paths. Travel times are displayed with a reduction velocity of 6.5 km/s. Pick uncertainties of the observed travel times are indicated by the heights of the vertical bars, calculated data are indicated by solid lines. OBS locations are marked by inverted triangles. Horizontal scale is distance (in km) for the velocity model of Fig. 6.

Figure 9: Free-air gravity anomaly map. The gravity data are taken from Oakey et al. (2001). Black lines show the location of the NUGGET refraction seismic experiment and the BGR/77-6 line; the position of the well Gjoa G-37 is marked by a red circle with a red dot in the middle. Gray lines show the position of the extinct spreading axis and faults, and dashed lines indicate magnetic anomalies (Roest and Srivastava 1989b). Thicker black line on line BGR/77-6 indicates profile shown in Fig. 12.

Figure 10: Updated geological map based on results from NUGGET Line 1 and 2. See legend for identification of map features. Original map is shown in Fig. 2 (from Chalmers and Pulvertaft 2001). Note the extension of basalt and underplating.

Figure 11: Velocity-depth curve of the southern part of Line 2 (solid line) and stacked velocity-depth curves (gray shading) for 59 to 127 Ma old oceanic crust in the Atlantic Ocean (White et al. 1992). Average oceanic crust is 7 km thick whereas the oceanic crust on Line 2 is 12 km thick.

Figure 12: Subset of record section from line BGR/77-6. Vertical scale is two-way travel time; horizontal scale is shotpoints. Distance scale bar is shown in top left corner. The cross point of Line 2 is marked at the top of the section. SDR: seaward-dipping reflections after Chalmers and Pulvertaft (2001).

Figure 13: (Top) Line drawing of the migrated multi-channel seismic line GreenCan Line 02-01 collected by TGS NOPEC. This line is coincident with Line 2. Vertical scale is two-way travel time; horizontal scale is the distance along the velocity model of NUGGET Line 2 (Fig. 6). The cross points of Line 1 and BGR/77-6 are marked at the top of the section. Gray lines indicate the layer boundaries of the velocity model. Details of reflection data within box.

(Bottom) Vertical scale is two-way travel time; horizontal scale is the distance along the velocity model of NUGGET Line 2 (Fig. 6). Shaded areas represent crustal types as observed in the velocity model and where obtained from time conversion of layer boundaries. The cross point with BGR line 77-6 is marked at the top of the section. Bold lines indicate seaward-dipping reflections (SDR).

Figure 14: Model for rifting and seafloor spreading in southern Davis Strait and northern Labrador Sea based on results from the NUGGET experiment. **a:** Continental rifting phase between Greenland and Labrador. **b:** Initial seafloor spreading (light grey shading). **c:** Basalt flows (dark gray) and underplating (medium gray). **d:** Seafloor spreading ended during chron 13 (34.8-33.3 Ma).

Table 1: Identification of layers in the velocity model, the name of the seismic phases and record sections on which they were identified.

Layer	Phase	OBS records for observed phases
Refractions in:		
Sediment layer 1	P_{s1}	1-9, 11, 14
Sediment layer 2	P_{s2}	1, 2, 4, 5, 9, 10, 15
Sediment layer 3	P_{s3}	1-6, 8
Sediment layer 4	P_{s4}	1, 2
Sediment layer 5	P_{s5}	1-7, 11-14
Basalt (+ sediments?)	P_{s6}	6, 8-15
Upper continental crust	P_{c1}	1-4
Lower continental crust	P_{c2}	1-5, 7
Oceanic layer 2	P_{L2}	4-15
Oceanic layer 3	P_{L3}	7-15
Underplating	P_{n1}	1, 2, 6, 7, 9
Upper mantle	P_{n2}	2-7, 10-12, 14
Oceanic layer 3 (S-wave)	S_{L3}	10-14
Reflections at:		
Base of upper continental crust	$P_{c1}P$	4, 6
Base lower continental crust	$P_{m1}P$	1-8
Base of oceanic layer 2	$P_{L2}P$	8
Base of oceanic layer 3	$P_{m3}P$	8-15
Base of underplating	$P_{m2}P$	7, 9
In the upper mantle	P_zP	2-4, 6, 8-12, 14
Base of oceanic layer 3 (S-wave)	S_mS	10-12, 14-15

Table 2: The number of travel time picks, the assigned pick uncertainty, the RMS (root-mean-squares) travel time residual, and the normalized χ^2 for individual *P*-phases.

Phase	Number of Observations	Average Pick Uncertainty, ms	RMS Misfit, ms	Normalized χ^2
Direct	1424	50	63	1.588
P_{S1}	178	57	49	0.787
P_{S2}	83	49	34	0.773
P_{S3}	111	62	60	0.878
P_{S4}	41	51	49	0.781
P_{S5}	196	83	80	0.954
P_{S6}	612	78	80	0.760
P_{c1}	500	70	77	0.868
P_{c2}	1369	79	75	1.023
P_{L2}	750	69	64	0.879
P_{L3}	3216	63	61	0.881
$P_{c1}P$	91	89	73	0.612
$P_{L2}P$	15	60	52	1.011
$P_{m1}P$	2165	100	92	0.808
$P_{m2}P$	473	88	84	0.900
$P_{m3}P$	1550	87	81	0.829
P_{n1}	712	112	97	0.800
P_{n2}	2177	111	99	0.773
P_zP	1503	139	174	0.817
Total	17175	95	92	0.908

Table 3: The number of travel time picks, the assigned pick uncertainty, the RMS (root-mean-squares) travel time residual, and the normalized χ^2 for individual *S*-phases.

Phase	Number of Observations	Average Pick Uncertainty, ms	RMS Misfit, ms	Normalized χ^2
S_{L3}	808	139	135	0.810
S_mS	651	139	176	1.380
Total	1459	139	155	1.064

Fig. 1

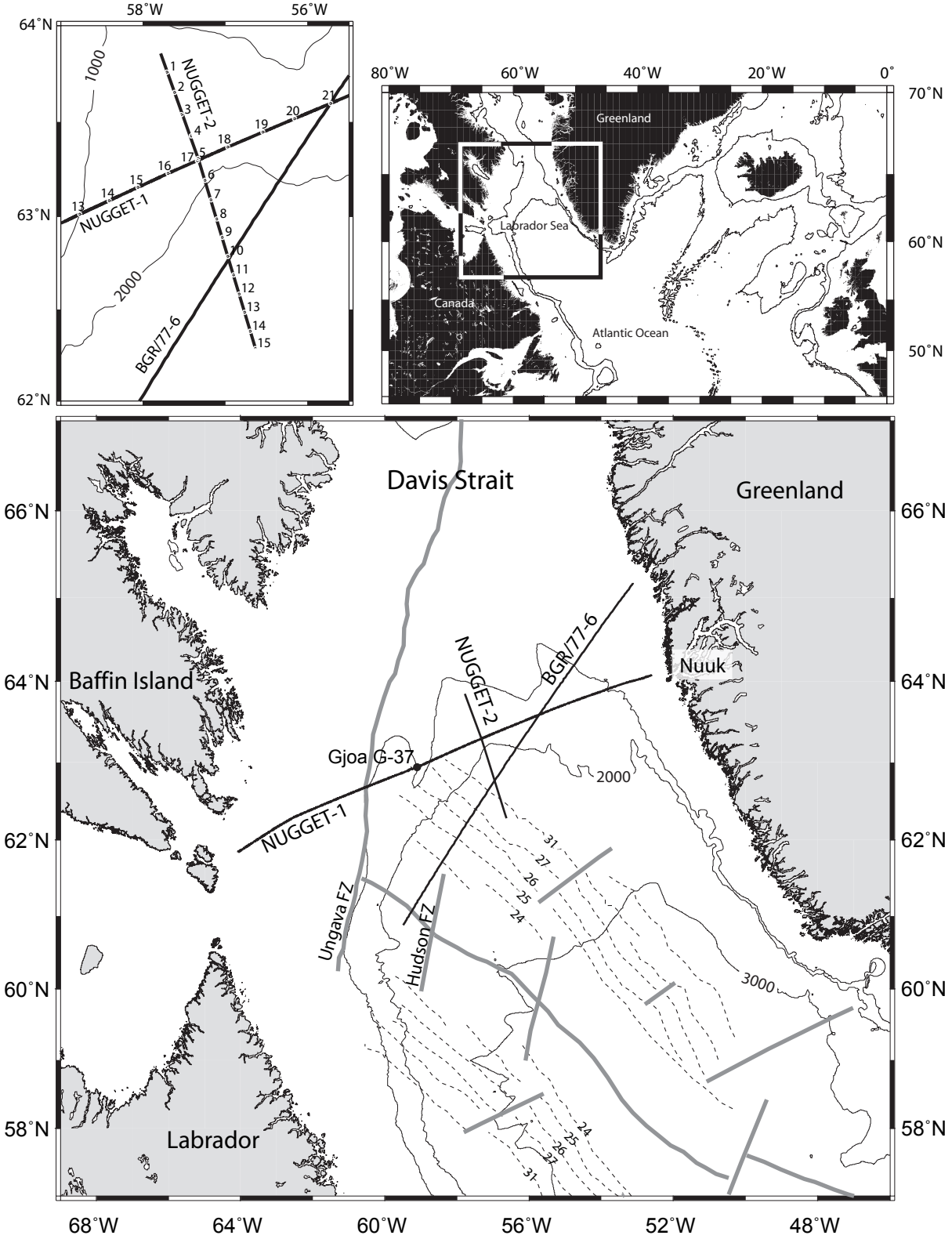
58°W
56°W
64°N
63°N
62°N
1000
2000
NUGGET-2
NUGGET-1
BGR/77-6
1
2
3
4
5
6
7
8
9
10
11
12
13
14
15
16
17
18
19
20
21
80°W
60°W
40°W
20°W
0°
70°N
60°N
50°N
Greenland
Labrador Sea
Canada
Atlantic Ocean
Davis Strait
Greenland
66°N
64°N
62°N
60°N
58°N
Baffin Island
Nuuk
Gjoa G-37
2000
3000
Ungava FZ
Hudson FZ
31
27
26
25
24
Labrador
68°W
64°W
60°W
56°W
52°W
48°W

Fig. 2

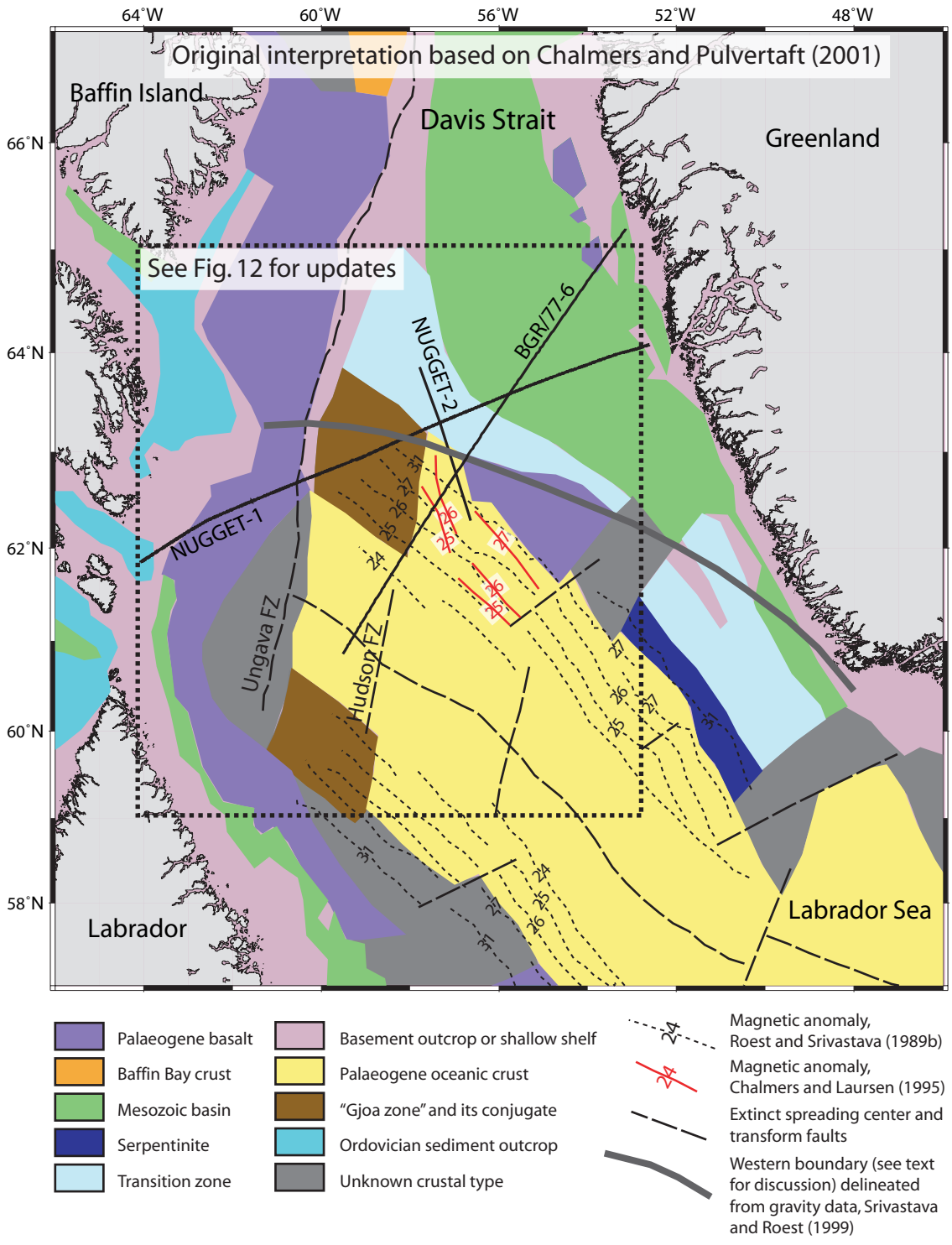
64°W
60°W
56°W
52°W
48°W
66°N
64°N
62°N
60°N
58°N
Original interpretation based on Chalmers and Pulvertaft (2001)
Baffin Island
Davis Strait
Greenland
See Fig. 12 for updates
NUGGET-2
BGR/77-6
NUGGET-1
Ungava FZ
Hudson FZ
Labrador
Labrador Sea
Palaeogene basalt
Baffin Bay crust
Mesozoic basin
Serpentinite
Transition zone
Basement outcrop or shallow shelf
Palaeogene oceanic crust
"Gjoa zone" and its conjugate
Ordovician sediment outcrop
Unknown crustal type
Magnetic anomaly, Roest and Srivastava (1989b)
Magnetic anomaly, Chalmers and Laursen (1995)
Extinct spreading center and transform faults
Western boundary (see text for discussion) delineated from gravity data, Srivastava and Roest (1999)

Fig. 3

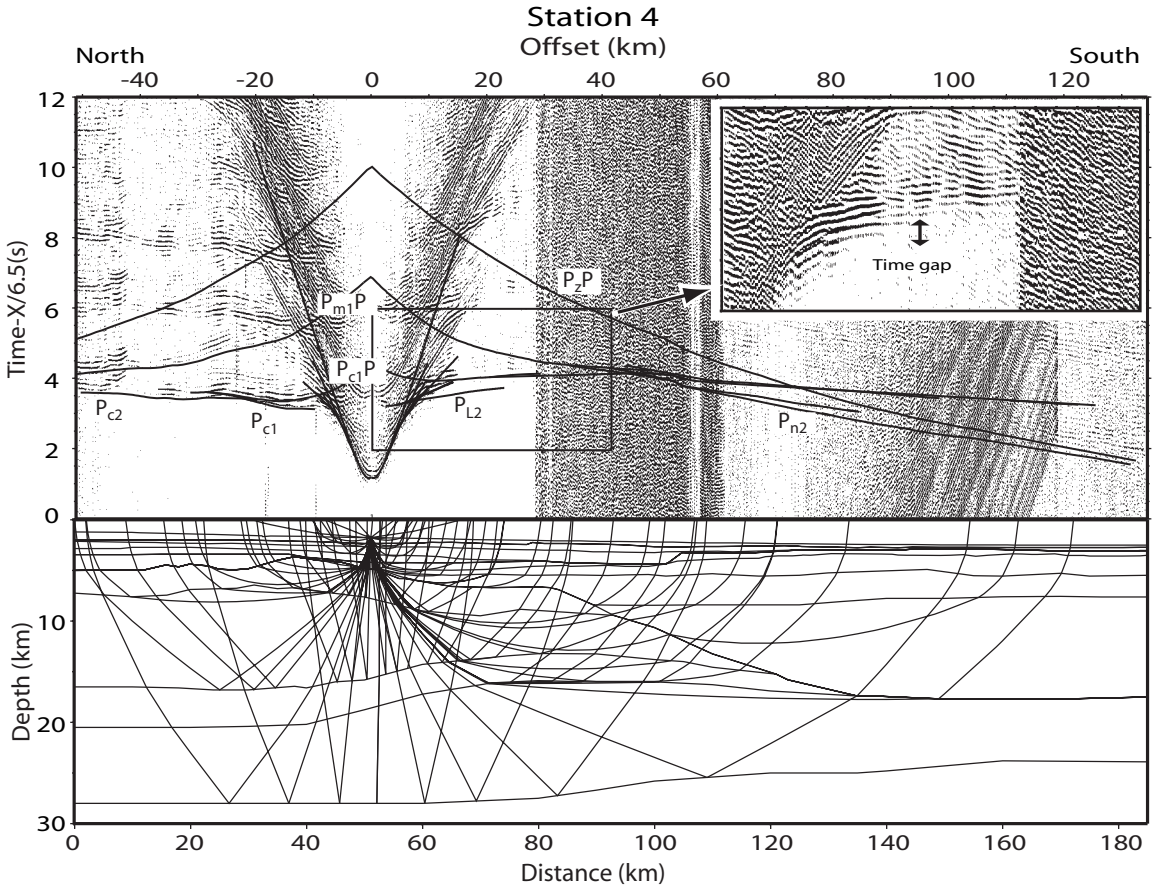
Station 4
Offset (km)
North
South
-40
-20
0
20
40
60
80
100
120
Time-X/6.5(s)
12
10
8
6
4
2
0
$P_{m1}P$
P_zP
$P_{c1}P$
P_{c2}
P_{c1}
P_{L2}
P_{n2}
Time gap
Depth (km)
10
20
30
0
20
40
60
80
100
120
140
160
180
Distance (km)

Fig. 4

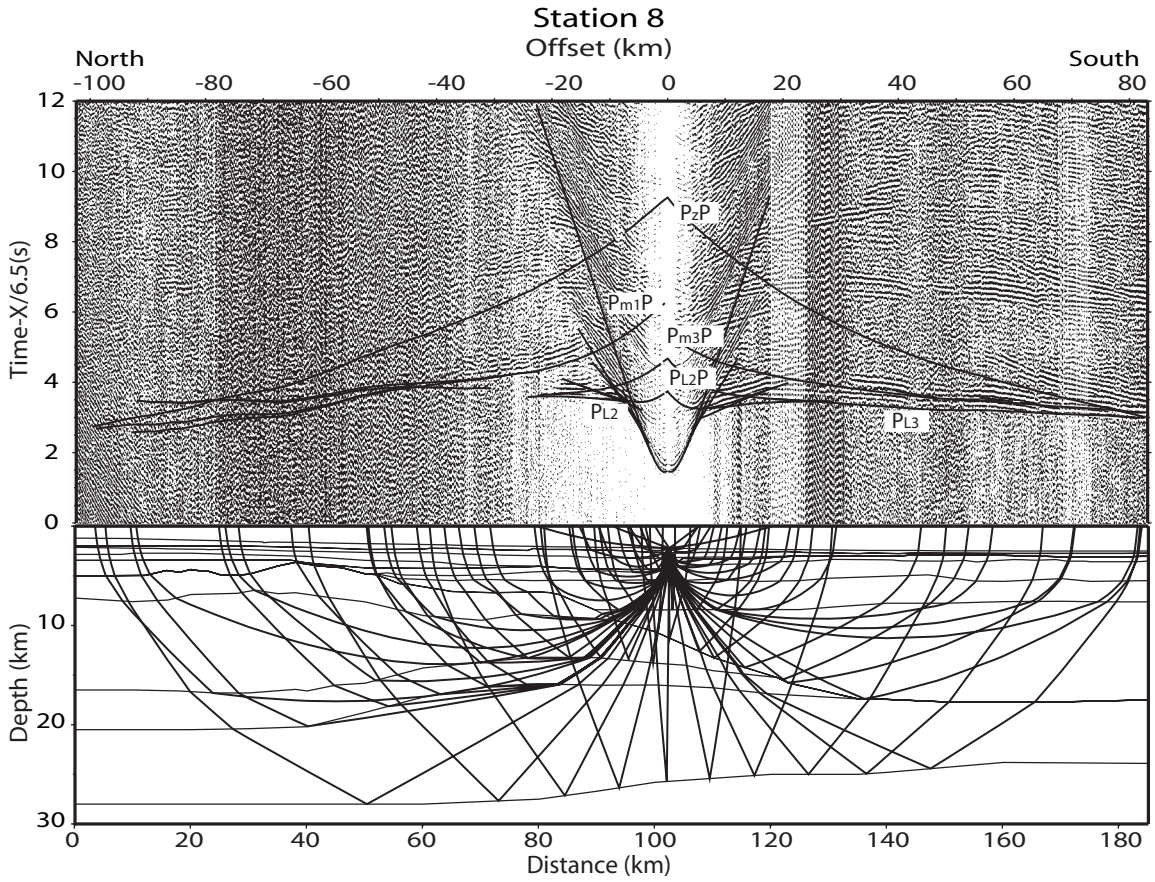
Station 8
Offset (km)
North
South
-100
-80
-60
-40
-20
0
20
40
60
80
Time-X/6.5(s)
12
10
8
6
4
2
0
PzP
Pm1P
Pm3P
PL2P
PL2
PL3
Depth (km)
10
20
30
0
20
40
60
80
100
120
140
160
180
Distance (km)

Fig. 5

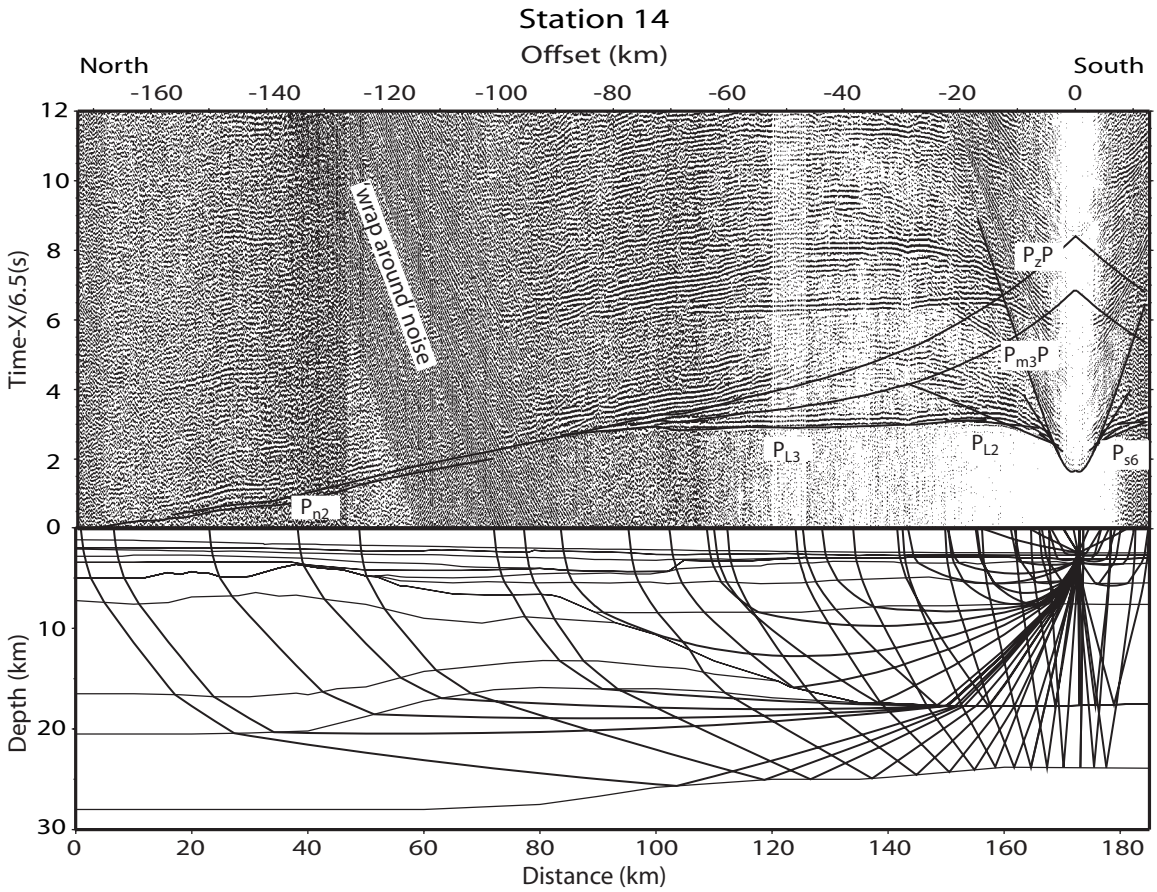
Station 14
Offset (km)
North
South
-160
-140
-120
-100
-80
-60
-40
-20
0
Time-X/6.5(s)
12
10
8
6
4
2
0
wrap around noise
P_zP
P_m3P
P_L3
P_L2
P_s6
P_n2
Depth (km)
0
10
20
30
0
20
40
60
80
100
120
140
160
180
Distance (km)

Fig. 6

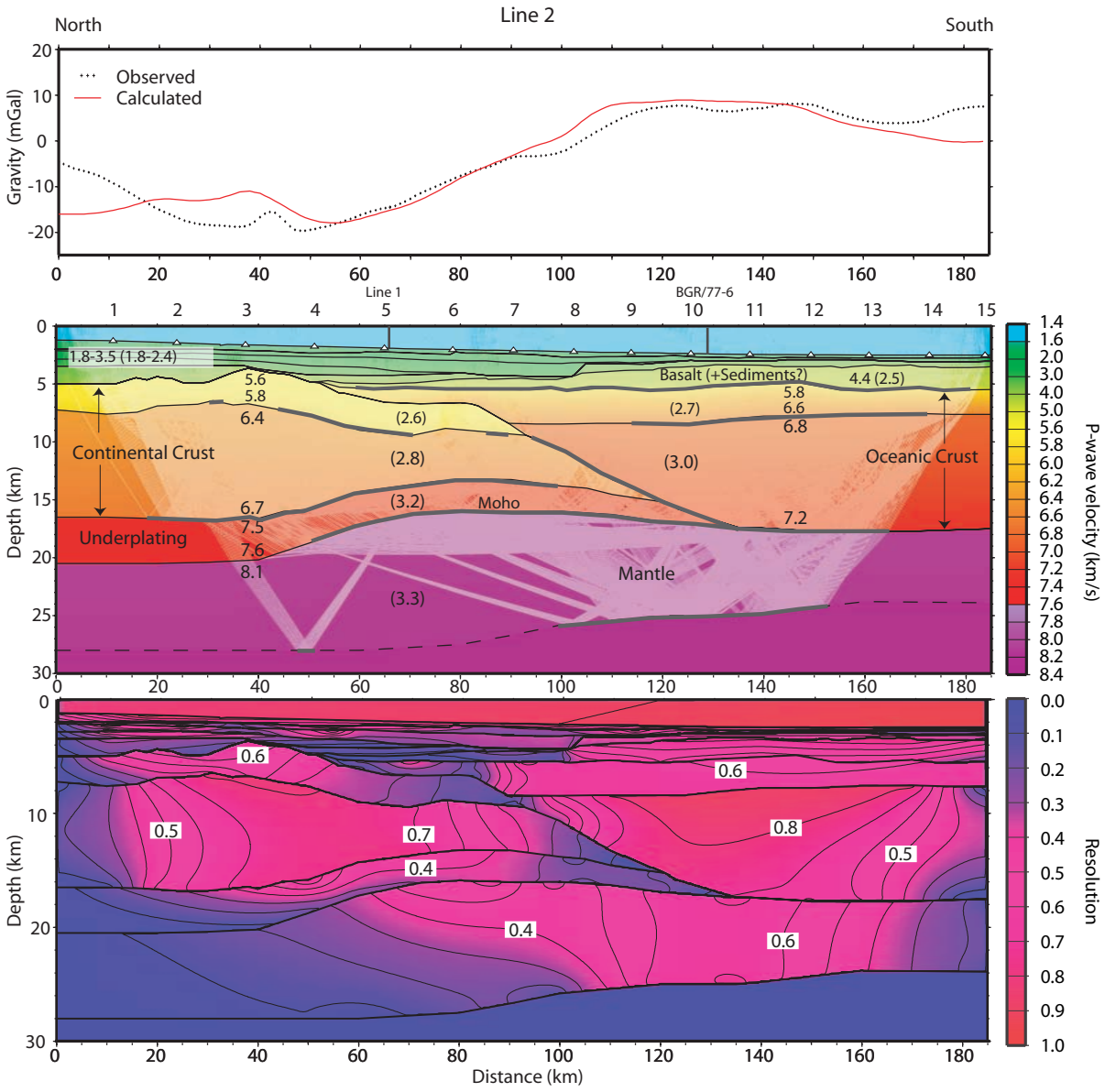
Line 2
North
South
Observed
Calculated
Gravity (mGal)
Line 1
BGR/77-6
1.8-3.5 (1.8-2.4)
Basalt (+Sediments?)
4.4 (2.5)
Continental Crust
Oceanic Crust
Underplating
Moho
Mantle
(2.6)
(2.7)
(2.8)
(3.0)
(3.2)
(3.3)
5.6
5.8
6.4
6.7
7.5
7.6
8.1
7.2
6.6
6.8
Depth (km)
Distance (km)
P-wave velocity (km/s)
Resolution
0.6
0.5
0.7
0.4
0.8

Fig. 7

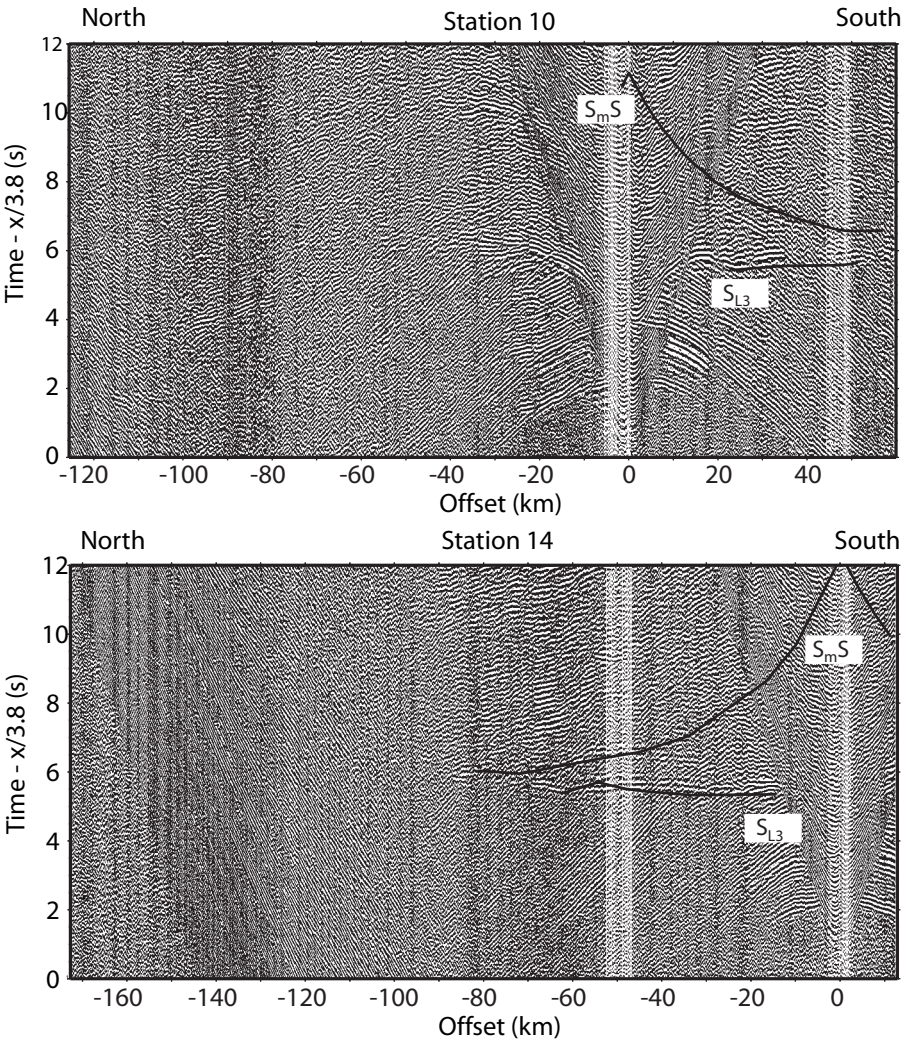
North
Station 10
South
Time - x/3.8 (s)
S_mS
S_{L3}
Offset (km)
North
Station 14
South
Time - x/3.8 (s)
S_mS
S_{L3}
Offset (km)

Fig. 8

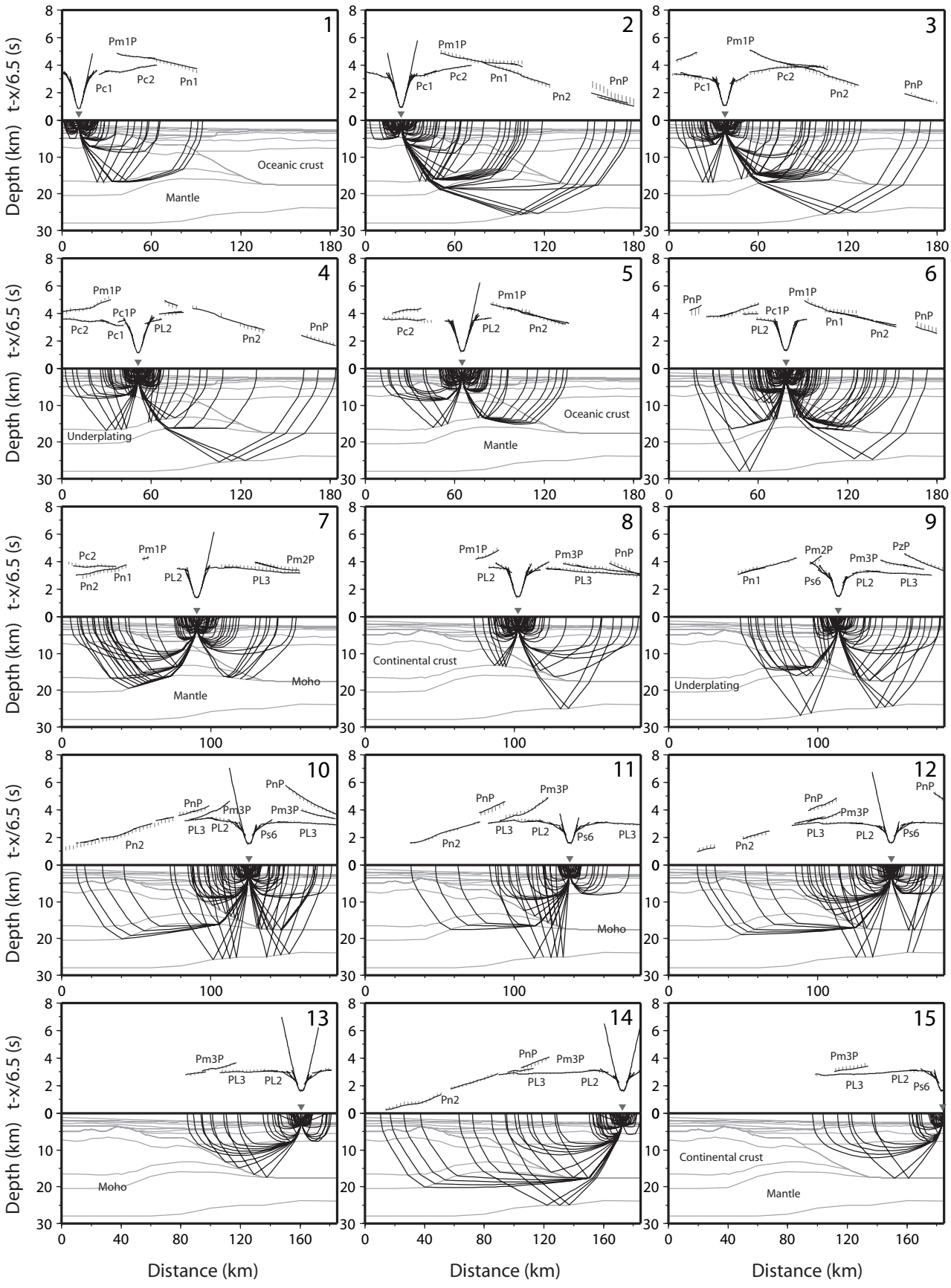
1
Pm1P
Pc1
Pc2
Pn1
Oceanic crust
Mantle
2
Pm1P
Pc1
Pc2
Pn1
Pn2
PnP
3
Pm1P
Pc1
Pc2
Pn2
PnP
4
Pm1P
Pc1P
Pc2
Pc1
PL2
Pn2
PnP
Underplating
5
Pm1P
Pc2
PL2
Pn2
Oceanic crust
Mantle
6
PnP
Pm1P
Pc1P
PL2
Pn1
Pn2
PnP
7
Pc2
Pm1P
Pn2
Pn1
PL2
Pm2P
PL3
Mantle
Moho
8
Pm1P
Pm3P
PnP
PL2
PL3
Continental crust
9
Pm2P
PzP
Pm3P
Pn1
Ps6
PL2
PL3
Underplating
10
PnP
PnP
Pm3P
Pm3P
PL3
PL2
Pn2
Ps6
PL3
11
PnP
Pm3P
PL3
PL2
Pn2
Ps6
PL3
Moho
12
PnP
PnP
Pm3P
PL3
PL2
Pn2
Ps6
13
Pm3P
PL3
PL2
Moho
14
PnP
Pm3P
PL3
PL2
Pn2
15
Pm3P
PL3
PL2
Ps6
Continental crust
Mantle
Depth (km) t-x/6.5 (s)
Distance (km)

Fig. 9

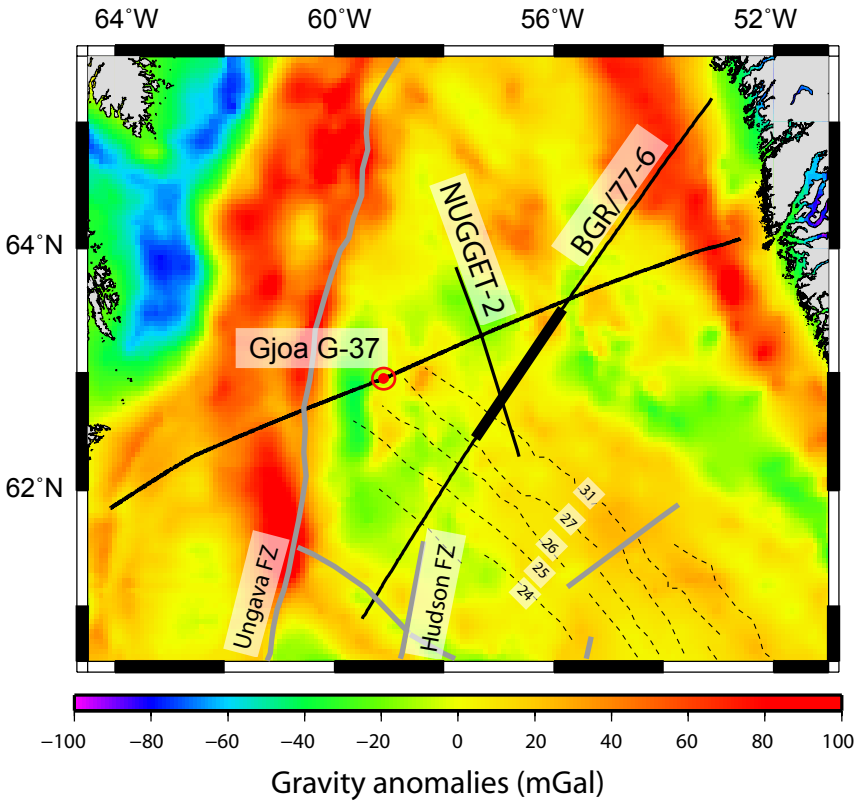
64˚W
60˚W
56˚W
52˚W
64˚N
62˚N
NUGGET-2
BGR/77-6
Gjoa G-37
Ungava FZ
Hudson FZ
31
27
26
25
24
−100
−80
−60
−40
−20
0
20
40
60
80
100
Gravity anomalies (mGal)

Fig. 10

Proposed modifications to the interpretation of Chalmers and Pulvertaft (2001)

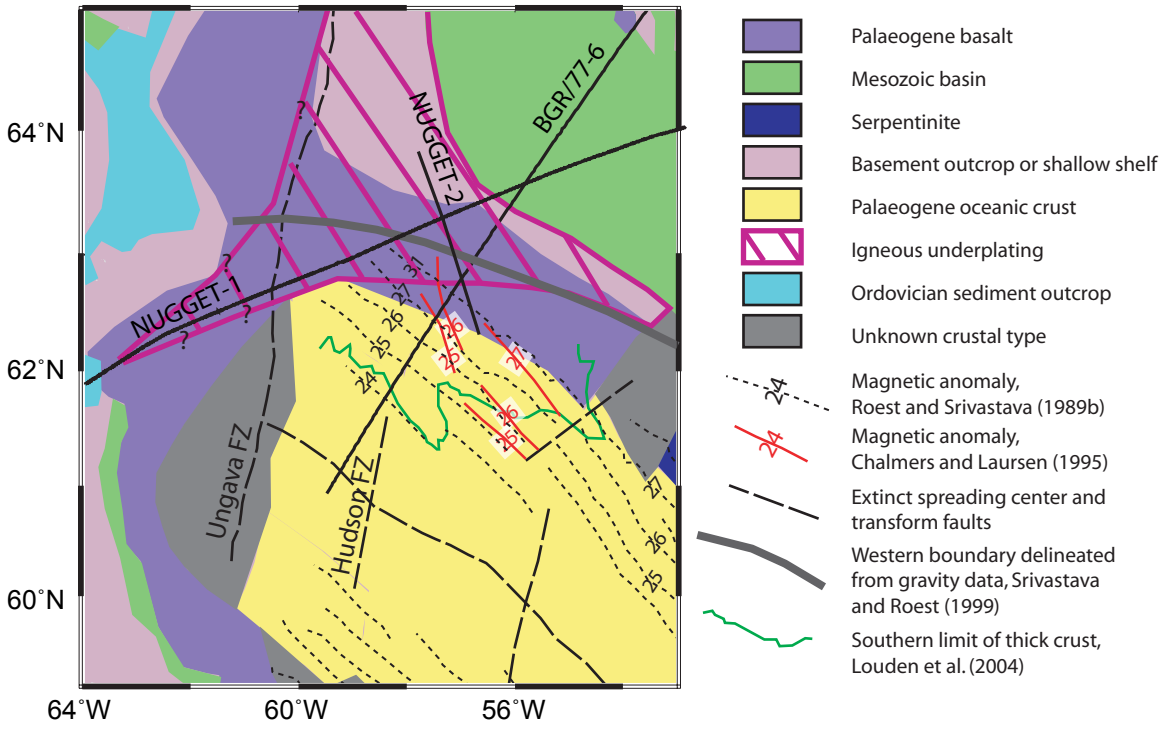

Fig. 11

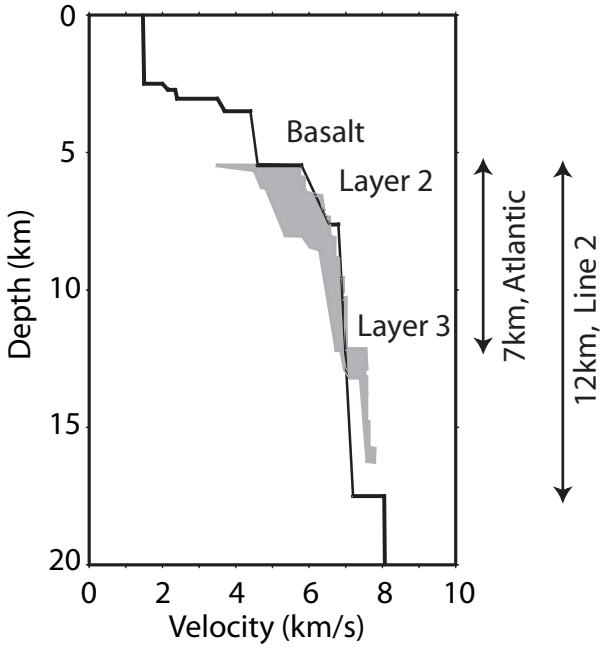
0
5
10
15
20
Depth (km)
0
2
4
6
8
10
Velocity (km/s)
Basalt
Layer 2
Layer 3
7km, Atlantic
12km, Line 2

Fig. 12

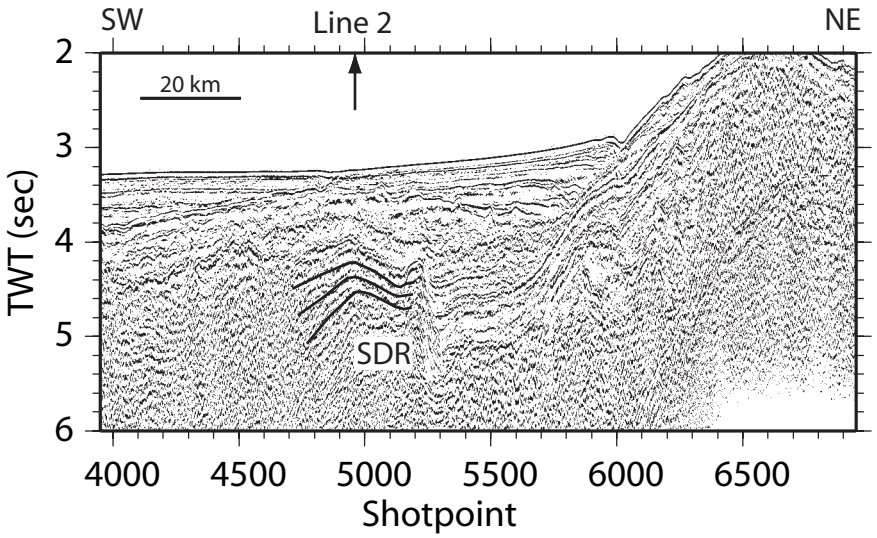
SW
Line 2
NE
20 km
TWT (sec)
2
3
4
5
6
SDR
4000
4500
5000
5500
6000
6500
Shotpoint

Fig. 13

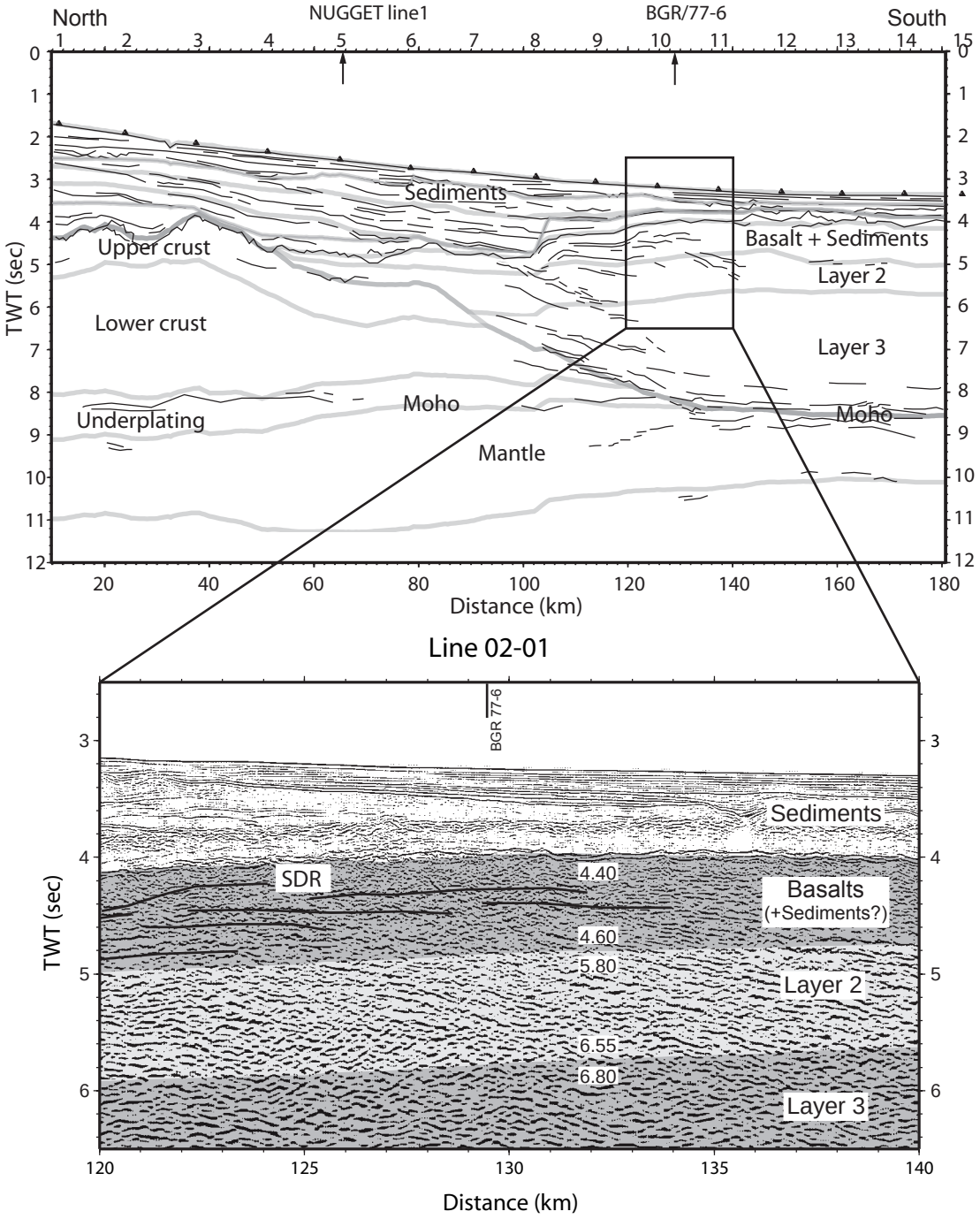
North
NUGGET line1
BGR/77-6
South
TWT (sec)
Distance (km)
Sediments
Upper crust
Lower crust
Underplating
Moho
Mantle
Basalt + Sediments
Layer 2
Layer 3
Moho
Line 02-01
BGR 77-6
Sediments
SDR
4.40
Basalts
(+Sediments?)
4.60
5.80
Layer 2
6.55
6.80
Layer 3
TWT (sec)
Distance (km)

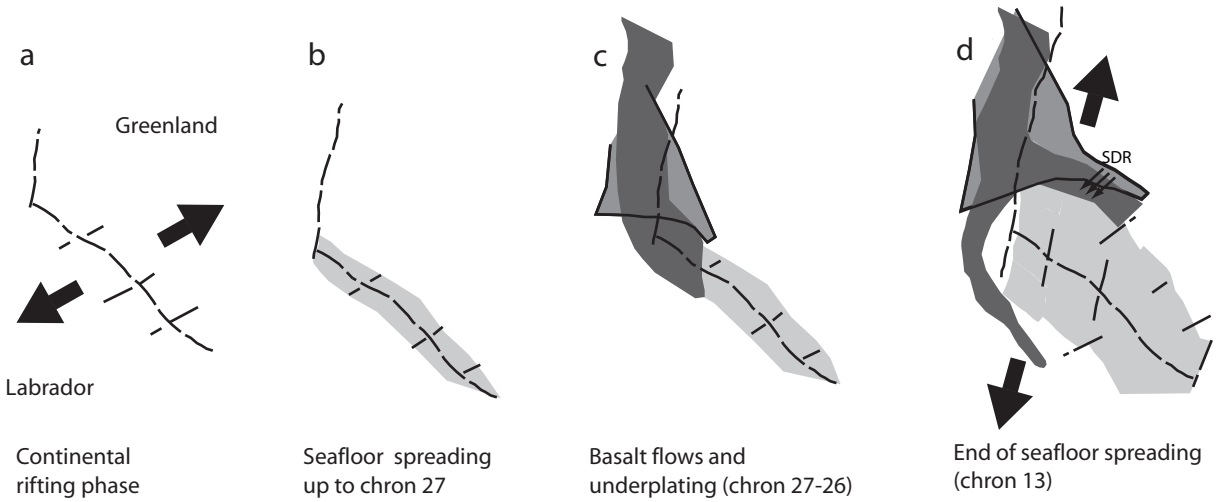

Continental rifting phase

Seafloor spreading up to chron 27

Basalt flows and underplating (chron 27-26)

End of seafloor spreading (chron 13)